CrystEngComm

Accepted Manuscript

ROYAL SOCIETY OF CHEMISTRY

www.rsc.org/crystengcomm

Cite this: DOI: 10.1039/c0xx00000x

www.rsc.org/xxxxxx

ARTICLE TYPE

Lanthanide coordination frameworks constructed from 2-amino-1,4-benzenedisulfonate, oxalate and 1, 10-phenanthroline: Crystal structure, down- and up-conversion luminescence and white light emission

Yi-Hua Zhang, Xia Li,* Shuang Song, Hong-Yu Yang, Dou Ma and Yi-Heng Liu

Received (in XXX, XXX) Xth XXXXXXXXX 20XX, Accepted Xth XXXXXXXXX 20XX
DOI: 10.1039/b000000x

The lanthanide−organic frameworks (LnOFs), $[Sm(H_2N\text{-}BDS)_{0.5}(ox)(phen)]$ (**1**) and $[Ln(H_2N\text{-}BDS)(ox)_{0.5}(phen)_2]$ (Ln = Eu **2**, Gd **3**, Tb **4**, Er **5**, Yb **6**; H_2N-BDS = 2-amino-1,4-benzenedisulfonate, ox = oxalate, and phen = 1, 10-phenanthroline) were obtained by hydrothermal syntheses. Structural analyses reveal that **1** is a three-dimensional (3D) pillared-layer structure constructed by $[SmO_6N_2]$ polyhedra, and tetradentate H_2N-BDS and tetradentate ox ligands, while complexes **2-6** are isostructural 2D frameworks, constructed by $[LnO_4N_4]$ polyhedra and bidentate H_2N-BDS and tetradentate ox ligands. LnOFs containing Sm(III), Eu(III) and Tb(III) ions exhibit the characteristic down- conversion luminescence of the corresponding Ln(III) ion. Gd:Tb,Eu doped complex provides a white light emission. Gd:Yb,Er doped complex exhibits up-conversion emission at 410 nm ($^4H_{9/2}\rightarrow {}^4I_{15/2}$, blue), 518–570 nm ($^4S_{3/2}$, $^2H_{11/2}\rightarrow {}^4I_{15/2}$, green), and 655 nm ($^4F_{9/2}\rightarrow {}^4I_{15/2}$, red).

1. Introduction

The lanthanide - organic frameworks (LnOFs) are a very active field in material chemistry and structural chemistry owing to the wide range of potential applications in bioassays, sensor systems and optical materials, etc.[1] Lanthanide ions exhibit sharp emission in the visible and near-infrared regions, line-like, long luminescent lifetime, and large Stokes shift. Furthermore, the emissive performance of LnOFs can be improve by doping other Ln(III) ions.[2] Among the Ln(III) ions, Gd(III) ion with $4f^7$ electronic configuration has the high energy of the lowest emitting level and is often employed as host material in the doped Ln(III) to achieve the desirable down-conversion (DC)[2a,b,c] or up-conversion (UC) luminescence[2j]. Eu(III) and Tb(III) ions emit intense red (616 nm) and green (545 nm) DC luminescence, respectively, which act as dopants in designing emitting materials to realize a multicoloured luminescence, including white light.[2a-i] White light emission based on metal - organic frameworks (MOFs) has been reported in recent years.[2a-h] White light emitting materials have broad applications in display and lighting. [2h,3] The Er(III) ion is a promising laser active ion for UC luminescence and the UC luminescence efficiency of Er(III) ion can be increased by codoping with Yb(III) ion. [4, 5] However, UC luminescence of lanthanide complexes is less studied[2j, 4c, 4d], which is mainly because the existence of multiphonon relaxation can decrease the efficiency of the process. UC luminescence materials have attracted significant attention as potential solid state visible lasers and biological labels[5].

The luminescent properties of lanthanide complexes strongly depend on the coordination sphere of the metal ion. The choice of ligand for the antenna effect plays a key role in constructing efficient lanthanide complexes. High-energy C-H, N-H, and O-H oscillators significantly quench the metal excited states nonradiatively, leading to decreased luminescence intensity.[6] Our strategy to obtain luminescent LnOFs with 2-amino-1,4-benzenedisulfonate (H_2N-BDS), 1, 10-phenanthroline (phen) and oxalate (ox) ligands. The rigid H_2N-BDS is a multidentate connector that allows for the formation of luminescent LnOFs. The complexes containing H_2N-BDS have been less explored to date.[7] It is well documented that phen can serve as both co-chelating and co-sensitizing ligand and it is helpful to enhance the luminescent property of complexes.[8] Ox anion can coordinate to Ln(III) ion to prevent water molecules binding to the Ln(III) ions, leading to a high luminescence intensity. Thus, a series of LnOFs, $[Sm(H_2N\text{-}BDS)_{0.5}(ox)(phen)]$ (**1**) and $[Ln(H_2N\text{-}BDS)(ox)_{0.5}(phen)_2]$ (Ln = Eu **2**, Gd **3**, Tb **4**, Er **5**, Yb **6**) were synthesized. Indeed, no water molecule exists in the coordination sphere of the Ln(III) ions. The Gd(III)-doping experiments by addition of the Eu/Tb, Yb/Er ions were carried out. Interestingly, white light emission is realized based on Gd:Tb,Eu doped complex by regulating the intensities of blue, green and red emissions in the doped complex. Gd:Yb,Er doped complex exhibits UC emission at 410 (blue), 518–570 (green), and 655 nm (red).

2. Experimental Section

2.1 Materials and Physical measurement

Lanthanide nitrates were prepared by the corresponding oxide with nitric acid. Other reagents were commercially available and were used without further purification. Infrared (IR) spectra were measured on a Bruker Tensor37 spectrophotometer using the KBr

pellets technique. Elemental analyses (C, H and N) were performed on an Elementar Vario EL analyzer. Inductively coupled plasma (ICP) spectroscopy was performed on an Agilent 7500Ce spectrometer. X-ray diffraction was carried out on a PANaytical X'Pert PRO MPD diffractometer for Cu Kα radiation (λ = 1.5406 Å), with a scan speed of 2°·min^{-1} and a step size of 0.02° in 2θ. The simulated PXRD patterns were obtained from the single-crystal X-ray diffraction data. Solid state fluorescence spectra were recorded on an FL4500 fluorescence spectrophotometer (Japan Hitachi company) at room temperature in identical operating conditions. The lifetimes were measured at room temperature on FLS920 Steady State & Time-resolved Fluorescence Spectrometer (Edinburgh Instrument). The emission quantum yields were measured at room temperature using a Quantum Yield Measurement System Fluorolog®-3 (HORIBA company) with a 450W Xe lamp coupled to a monochromator for wavelength discrimination, an integrating sphere as sample chamber, and an analyzer R928P for signal detection. Up-conversion spectrum was obtained with a Hitachi F4500 fluorescence spectrophotometer with an external 980 nm excitation source (Beijing Hi-Tech Optoelectronic Co., China) instead of the xenon source in the spectrophotometer and with a fiber-optic accessory. Thermogravimetric analyses (TGA) were carried out using a shimadzu DTG-60AH thermal analyzer (Japan) under air from room temperature to 800 °C with a heating rate of 10 °C/min.

2.2. Synthesis of complexes 1-6

A mixture of $Ln(NO_3)_3·6H_2O$ (0.1 mmol) (Ln = Sm **1**, Eu **2**, Gd **3**, Tb **4**, Er **5**, Yb **6**), 2-amino-1,4-benzenedisulfonate (0.2 mmol), oxalate (0.1 mmol), 1, 10-phenanthroline (0.2 mmol), H_2O (10 mL), and an aqueous solution of NaOH (1 mol/L, 0.20 mL) was sealed in a Teflon-lined reactor and heated at 140 °C for 3 days. After slow cooling to room temperature, block crystals of the complexes were obtained. Yield: about 65% based on the Ln(III). For **1**: Anal. Calcd for $C_{34}H_{21}N_5O_{14}S_2Sm_2$: C, 37.52; N, 6.43; H, 1.94%. Found: C, 37.40; N, 6.31; H, 1.87%. Selected IR (KBr pellet, cm^{-1}): 1679(vs), 1608(vs), 1521(m), 1427(s), 1312(m), 1242(s), 1171(s), 1049(m), 1021(m), 889(w), 851(m), 792(m), 729(m), 663(s). For **2**: Anal. Calcd for $C_{31}H_{21}N_5O_8S_2Eu$: C, 46.10; N, 8.67; H, 2.62%. Found: C, 45.91; N, 8.19; H, 2.76%. Selected IR (KBr pellet, ν/cm^{-1}): 1651(vs), 1520(m), 1426(s), 1314(s), 1261(s), 1166(s), 1102(s), 863(m), 844(m), 797(m), 724(s), 666(s). For **3**: Anal. Calcd for $C_{31}H_{21}N_5O_8S_2Gd$: C, 45.80; N, 8.61; H, 2.60%. Found: C, 45.05; N, 8.49; H, 2.72%. Selected IR (KBr pellet, cm^{-1}): 1650(vs), 1519(m), 1425(s), 1315(m), 1262(s), 1166(s), 1111(m), 1002(s), 863(m), 843(m), 797(m), 724(s), 665(s). For **4**: Anal.Calcd for $C_{31}H_{21}N_5O_8S_2Tb$: C, 45.71; N, 8.60; H, 2.60%. Found: C, 45.35; N, 8.47; H, 2.69%. Selected IR (KBr pellet, cm^{-1}): 1650(vs), 1519(m), 1425(s), 1316(m), 1261(s), 1166(s), 1110(m), 1003(s), 863(m), 843(m), 797(m), 724(s), 665(s). For **5**: Anal.Calcd for $C_{31}H_{21}N_5O_8S_2Er$: C, 45.25; N, 8.51; H, 2.57%. Found: C, 45.15; N, 8.43; H, 2.60%. Selected IR (KBr pellet, cm^{-1}): 1655(vs), 1520(m), 1425(s), 1317(m), 1264(s), 1167(s), 1111(m), 1005(s), 863(m), 843(m), 798(m), 725(s), 665(s). For **6**: Anal.Calcd for $C_{31}H_{21}N_5O_8S_2Yb$: C, 44.93, N, 8.45, H, 2.55%. Found: C, 45.01; N, 8.39; H, 2.52%. Selected IR (KBr pellet, cm^{-1}): 1652(vs), 1523(m), 1427(m), 1319(m), 1262(s) 1166(s), 1110(m), 1004(s), 864(m), 843(m), 798(m), 725(s), 666(s). For $Gd_{77.82}Eu_{9.92}Tb_{12.26}$ doped complex: Found: 45.73, N, 8.70, H, 2.79%. Selected IR (KBr pellet, cm^{-1}): 1629(vs), 1520(m), 1426(s), 1315(s), 1261(s), 1167(s), 1106(s), 1002(s), 853(m), 844(m), 797(s), 726(s), 666(s). For $Gd_{90.52}Yb_{5.89}Er_{3.59}$: Found: C, 45.11; N, 8.60; H, 2.74%. Selected IR (KBr pellet, cm^{-1}): 1629(vs), 1520(m), 1426(s), 1316(m), 1264(s), 1168(s), 1106(m), 1004(s), 853(m), 843(m), 778(m), 727(s), 668(s).

2.3. X-ray crystal structure determination

The X-ray single crystal data collections for the six complexes were performed on a Bruker Smart Apex II CCD diffractometer equipped with a graphite monochromated Mo Kα radiation (λ = 0.71073 Å) at 293(2) K. Semiempirical absorption correction was applied on the complexes using the SADABS program. The structures were solved by direct methods and refined by full matrix least squares method on F^2 using SHELXS 97 and SHELXL 97 programs.[9] All non-hydrogen atoms in the complexes were refined anisotropically. The hydrogen atoms were generated geometrically and treated by a mixture of independent and constrained refinement. A summary of the crystallographic data and details of the structure refinements are listed in **Table 1**. The selected bond lengths and bond angles are listed in **Table S1**.

3. Results and Discussion

3.1 Crystal Structure

Structure of $[Sm(H_2N\text{-}BDS)_{0.5}(ox)(phen)]$ (**1**). The asymmetric unit of **1** comprises one Sm(III) ion, half piece of H_2N-BDS ligand, two half pieces of ox and phen ligands. The oxalate moieties and the H_2N-BDS ligand lie about inversion centres in the crystal structure The coordination environment around Sm(III) is a distorted $[SmO_6N_2]$ square antiprism by two oxygen atoms (O3 and O4B) from two H_2N-BDS ligands, four oxygen atoms (O1, O2A, O6, and O7C) from two ox ligands, and two nitrogen atoms (N1 and N2) from phen molecule (Fig. 1a). The Sm1-O (sulfonate) distances are 2.394(4) and 2.399(3) Å. The Sm1-N distances are 2.572(3) and 2.580(4) Å. The Sm1-O (ox) distances range from 2.399(3) to 2.437(3) Å. The sulfonate groups of H_2N-BDS and carboxylate groups of ox exhibit only a bridging-bidentate coordination mode. H_2N-BDS ligand is considered as a connector between four Sm(III) ions while ox ligand is considered as a connector between two Sm(III) ions. Sm(III) ions are connected by ox linkers giving rise to Sm-ox zigzag chains with Sm…Sm separation of 6.296 Å. The Sm-ox chains show double-stranded helices consisting of the right- and left-handed helices sharing the Sm(III) ions along the b-axis. The chains are cross-linked through SO_3 groups, leading to a layer with Sm…Sm of 5.963 Å on the ab-plane. Interestingly, the layer also consists of right- and left-handed double-stranded helices along the b-axis. Each turn of the helix contains four ox ligands, two SO_3 groups and six Sm(III) ions with a pitch of 19.277 Å (Fig. 1b). The linear H_2N-BDS linkers connect the layers to form a pillared-layer 3D framework, giving Sm…Sm distance of 10.013 Å across the columns running along the c axis (Fig. 1c). Topological analysis of this framework with TOPOS software [10] reveals a $\{3^6.4^8.5^6.6\}$ topology structure.

Table 1. Crystal data and structure refinement for complexes **1- 6**

Complex	**1**	**2**	**3**	**4**	**5**	**6**
Empirical formula	$C_{34}H_{21}N_5O_{14}S_2Sm_2$	$C_{31}H_{21}N_5O_8S_2Eu$	$C_{31}H_{21}N_5O_8S_2Gd$	$C_{31}H_{21}N_5O_8S_2Tb$	$C_{31}H_{21}N_5O_8S_2Er$	$C_{31}H_{21}N_5O_8S_2Yb$
Formula weight	1088.38	807.61	812.90	814.57	822.91	828.69
Crystal system	Triclinic	Triclinic	Triclinic	Triclinic	Triclinic	Triclinic
space group	$P\bar{1}$	$P\bar{1}$	$P\bar{1}$	$P\bar{1}$	$P\bar{1}$	$P\bar{1}$
a(Å)	9.6304(7)	10.551(2)	10.5440(14)	10.5381(14)	10.542(3)	10.5522(9)
b(Å)	9.6386(7)	10.620(2)	10.5785(15)	10.5712(13)	10.561(3)	10.5726(10)
c(Å)	10.0130(7)	15.094(4)	15.068(2)	15.041(2)	14.961(4)	14.9134(13)
α(°)	85.4430(10)	74.956(18)	92.469(3)	75.114(4)	75.527(6)	75.774(2)
β(°)	72.7850(10)	69.597(11)	110.420(2)	69.497(2)	69.711(6)	69.8350(10)
γ(°)	72.7610(10)	72.234(11)	107.942(3)	72.006(2)	71.721(6)	71.5590(10)
Volume ($Å^3$)	847.89(11)	1487.2(6)	1476.9(3)	1471.7(4)	1464.7(7)	1464.1(2)
Z	1	2	2	2	2	2
Calculated density / g· cm^{-3}	2.132	1.803	1.828	1.838	1.866	1.880
Absorption coefficient/ mm^{-1}	3.635	2.312	2.450	2.608	3.071	3.400
F(000)	528	802	804	806	812	816
Crystal size / mm^3	0.26x0.11x0.04	0.25x0.18x0.10	0.22x0.10x0.08	0.20x0.10x0.03	0.20x0.10x0.03	0.20x0.12x0.05
θ range for data collection / (°)	2.21 to 25.00	2.04 to 25.00	2.12 to 25.25	2.05 to 25.00	2.06 to 25.00	2.05 to 25.00
Limiting indices	-5≦h≦11; -11≦k≦11; -11≦l≦11	-12≦h≦12; -12≦k≦12; -17≦l≦17	-6≦h≦12; -12≦k≦12; -18≦l≦17	-12≦h≦12; -10≦k≦12; -17≦l≦17	-12≦h≦12; -10≦k≦12; -17≦l≦16	-11≦h≦12; -12≦k≦11; -15≦l≦17
Reflections collected/unique	[R(int)= 0.0197] 4228 / 2957	[R(int)= 0.1132] 15738 / 5226	[R(int)= 0.0480] 7454 / 5313	[R(int)= 0.0531] 7270/ 5147	[R(int)= 0.0927] 7307/ 5136	[R(int)= 0.0226] 7222/ 5119
Data / restraints / parameters	2957 / 36 / 277	5226 / 204 / 463	5313 / 198 / 463	5147 / 204 / 463	5136 / 210 / 463	5119 / 210 / 463
Goodness-of-fit on F^2	1.038	1.083	1.012	0.999	0.956	0.980
Final R indices[I>2sigma(I)]	R1 = 0.0253 wR2 =0.0607	R1 = 0.0568 wR2 =0.1280	R1 = 0.0568 wR2 =0.1091	R1 = 0.0583 wR2 =0.1155	R1 = 0.0818 wR2 =0.1494	R1 = 0.0333 wR2 =0.0811
R indices(all data)	R1 = 0.0280 wR2 = 0.0624	R1 = 0.0879 wR2 = 0.1412	R1 = 0.0827 wR2 =0.1215	R1 = 0.0875 wR2 =0.1308	R1 = 0.1437 wR2 =0.1837	R1 = 0.0393 wR2 =0.0849
Largest difference peak and hole / e.$Å^{-3}$	0.773 and -0.650	1.604 and -1.217	1.393 and -0.693	1.282 and -1.258	1.363 and -1.226	1.353 and -0.820
CCDC No.	981691	981692	981693	981694	981695	981696

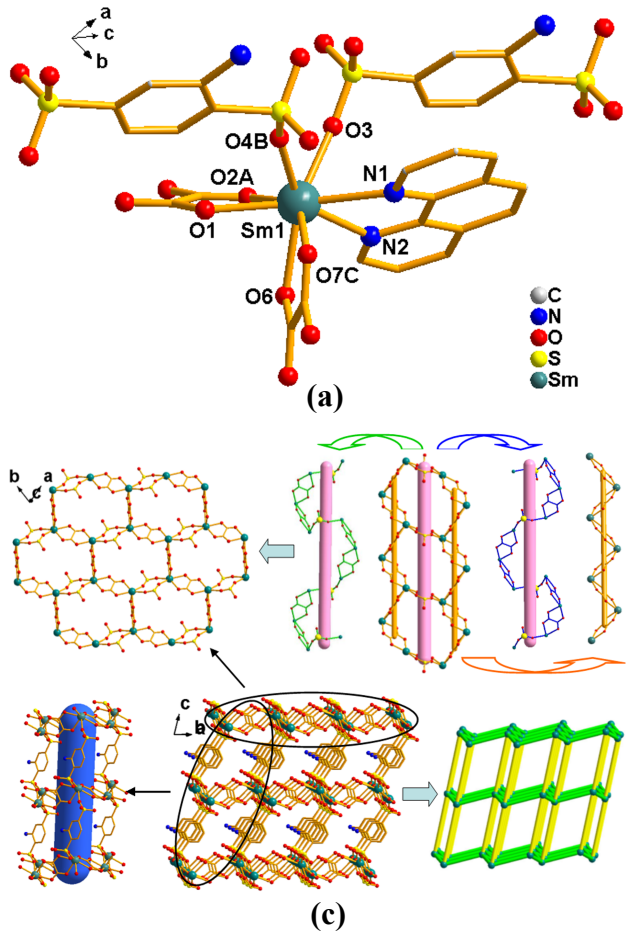

Fig. 1 View of the structure of **1**: (a) Coordination environment of Sm(III) ion. Symmetry codes: A: -x, -y, 1-z; B: 1-x, -y, 1-z; C: -x, 1-y, 1-z. (b) Layer constructed from the left- and right-hand helical Ln-ox and Ln- SO_3 –ox chains. Phen ligands are omitted for clarity. (c) A pillared-layer 3D framework.

Structure of [Ln(H_2N-BDS)$(ox)_{0.5}(phen)_2$] (Ln = Eu **2**, Gd **3**, Tb **4**, Er **5**, Yb **6**). The complexes **2**-**6** are isostructurs but different from **1** in both the compositions and structures. The complex **2** is selected as an example to describe the structure. The asymmetric unit of **2** comprises one Eu(III) ion, two half pieces of H_2N-BDS ligands, a half ox ligand, and two phen ligands. As in **1**, H_2N-BDS and ox ligands in the crystal structure of **2** also lie in the inversion centers. The coordination environment around Eu(III) is a distorted [EuO_4N_4] square antiprism by two oxygen atoms (O2 and O4) from two H_2N-BDS ligands, two oxygen atoms (O7A and O8) from ox, and four nitrogen atoms (N1, N2, N3, and N4) from two phen molecules (Fig. 2a). The Eu1-O (sulfonate) distances are 2.350(5) Å. The Eu1-N distances range from 2.556(6) to 2.588(7) Å. The Eu1-O (ox) distances are 2.345(5) and 2.395(5) Å. Different from **1**, H_2N-BDS ligand acting as linear linkers between two Eu(III) ions adopt a bis-monodentate coordination mode, while ox ligand serving as linear linker between two Eu(III) ions shows the same coordination mode as in 1.The two terminal phen molecules are not parallel with the dihedral angle of 84.10° . The H_2N-BDS ligands link two neighboring Eu(III) ions to form [Eu(H_2N-BDS)]n zigzag chains with the Eu…Eu…Eu angle of 144.56° .

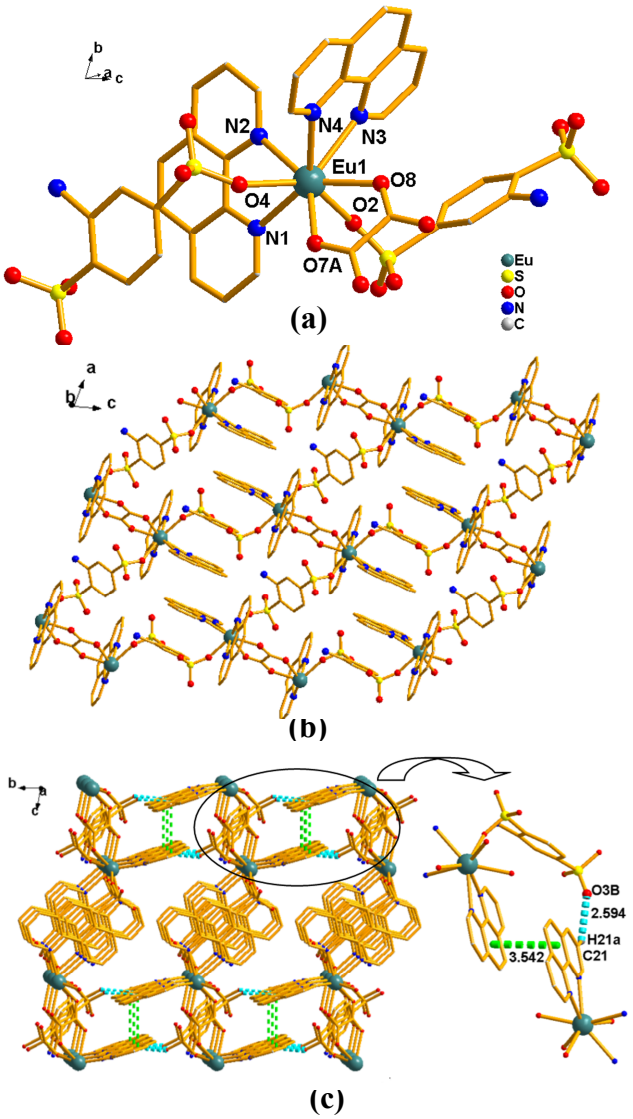

Fig. 2 View of the structure of **2**: (a) Coordination environment of Eu(III) ion. (b) 2D layer structure. (c) 3D supramolecular structure by C-H…O and π…π stacking interaction. Symmetry codes: A: -x, -y, 1-z. B: -1+x, 1+y, z.

The chains are conjoined through ox moieties into (6, 3) grid like layer running parallel to the ac crystal plane (Fig. 2b). The separations of Eu…Eu by ox and 2,6-NDS ligands are 7.164 and 21.218 Å, respectively. The layers stack in a parallel fashion (interlayer Eu–Eu distance of 10.620Å) along the a crystal direction and are pinned by noncovalent interactions. The C-H…O hydrogen bonds are present between phen molecule and sulfonate group [C21-H21a…O3B-S1, 3.192(5) Å]. The face–to-face π…π stacking interaction is found between the two phen molecules from neighboring layers with the centroid-centroid distance of 3.542 Å. So, 3D supramolecular structure is formed by the noncovalent interactions. (Fig. 2c)

Comparing the average distances (Table S1, ESI†) of the Ln-O, Ln-N, and Ln···Ln for the complexes **1**-**6**, the corresponding distances decrease as the ionic radius of the Ln(III) ions decrease in the order of Sm(III) > Eu(III) > Gd(III) > Tb(III) > Er(III) >Yb(III), which is consistent with the lanthanide contraction.

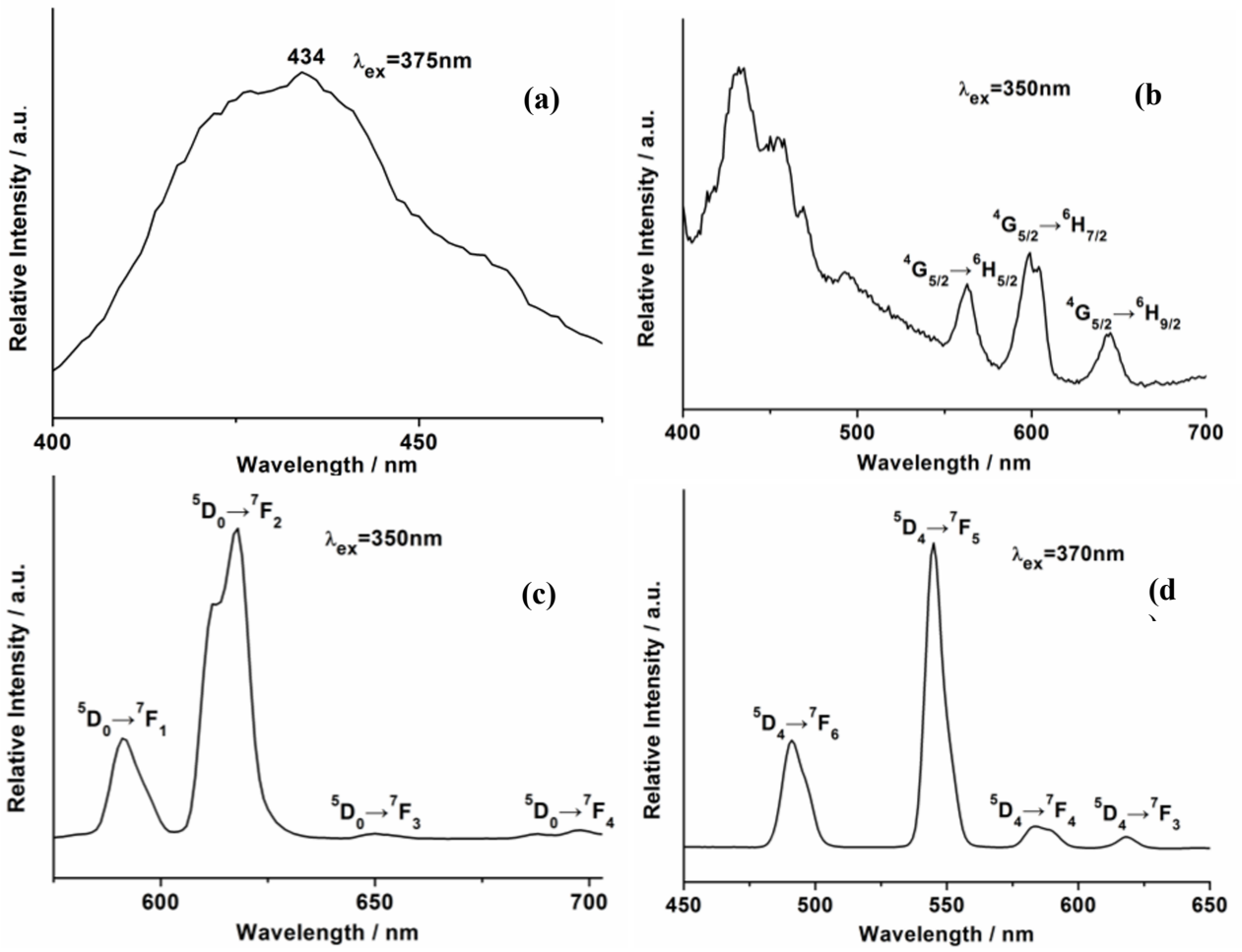

Fig. 3 Emission spectra of the complexes **3** (a), **1** (b), **2** (c), **4** (d) in the solid state at room temperature.

3.2 Luminescent Property

The luminescent properties of the complexes in the solid state were investigated at room temperature. Under excitation at 375 nm, complex **3** displays blue emission with the band centered at 434 nm (Fig. 3a).The band coincides with a ligand-based emission (446 nm for H_2N-BDS, 436 nm for phen and 432 nm for ox) (Fig. S2, ESI†), and may be attributed to the π*-π transitions of the ligands. Because the lowest excited state, $^6P_{7/2}$ of Gd(III) is too high (at around 32150 cm^{-1}) [11] to accept energy from the ligand, there is no Gd(III) f→f emission in the visible range. Upon excitation of 350 nm, complex **1** exhibits three emission bands at 563, 598, and 644 nm (Fig. 3b), which are attributed to $^4G_{5/2}\rightarrow\ ^6H_{5/2}$, $^4G_{5/2}\rightarrow\ ^6H_{7/2}$, and $^4G_{5/2}\rightarrow\ ^6H_{9/2}$ transitions of Sm(III) ion, respectively. A broad emission band centered at 434 nm is observed, which arises from the ligands[12]. The luminescent quantum yield is 2 %, and the luminescent lifetime is $\tau_1 = 0.008 \pm 0.00$ ms and $\tau_2 = 0.319 \pm 0.03$ ms (Fig. S3a, ESI†). Complexes **2** and **4** show a strong red and green luminescence upon irradiation with ultraviolet light, respectively. The excitation spectra were collected by monitoring the 617 nm for **2** and 544 nm for **4** (Fig. S4, ESI†). An intense broad bands centered at 350 nm for **2** and 370 nm for **4** correspond to the π-π* transition of ligands. The narrow band at 395 nm arises from $^7F_0\rightarrow{}^5L_6$ of Eu(III) ion for **2**. The intense ligand band indicates that luminescence sensitization via excitation of the ligands is effective for **2** and **4**. Upon excitation at 350 nm, the emission spectrum of **2** consists of characteristic $^5D_0\rightarrow{}^7F_J$ (J = 1−4) transitions at 591, 617, 650, and 698 nm, respectively (Fig. 3c). The strongest transition $^5D_0\rightarrow{}^7F_2$ is at 617 nm with a shoulder of 613 nm. The intensity ratio of 3.51 for $I(^5D_0\rightarrow{}^7F_2) : I(^5D_0\rightarrow{}^7F_1)$ indicates that Eu(III) ion does not locate on an inversion center. When excited at 370 nm, complex **4** gives characteristic Tb(III) emission at 490, 544, 584, and 619 nm, which are assigned to the transitions from the $^5D_4$ level to the ^7F_J (J = 6, 5, 4, 3) levels (Fig. 3d). The $^5D_4\rightarrow{}^7F_5$ emission is the most prominent one. No emission from the ligand could be observed in emission spectra **2** and **4**, which indicates that the ligands absorb and transfer energy efficiently to central Eu(III)/Tb(III) ions. In addition, the half-width of the strongest band is less than 10 nm, indicating that complexes **2** and **4** exhibit high fluorescence intensity and color purity. The luminescent lifetime for **2** and **4** was measured from the decay profile by fitting with biexponential decay curve with $\tau_1 = 0.336 \pm 0.06$ ms and $\tau_2 = 0.757 \pm 0.03$ ms for **2** and $\tau_1 = 0.069 \pm 0.02$ ms and $\tau_2 = 0.195 \pm 0.03$ ms for **4** (Fig. S3b,c, ESI†). The luminescent quantum yields for **2** and **4** are 3.62% and 9.10%, respectively. Complexes 1, 2, 4 show weak luminescence efficiency due to the quenching effect of high-energy C-H/N-H oscillators from the ligands and/or poor matching of the triplet state of the ligand with that of the emissive excited states of the

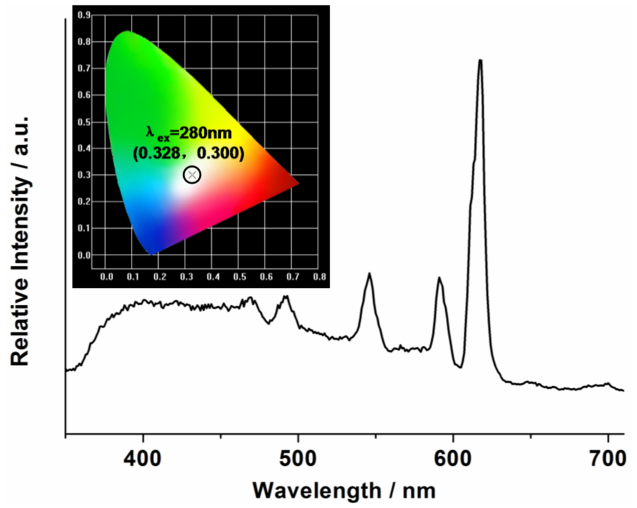

Fig. 4 Emission spectrum of the $Gd_{77.82}Eu_{9.92}Tb_{12.26}$ doped complex. Inset: The CIE chromaticity diagram.

Ln(III) ion. However, the luminescence lifetimes and quantum yields are comparable to the reported ones of the LnOFs[13].

The emissions of Eu(III), Tb(III), and Gd(III)- complexes locate at the red, green, and blue regions, respectively. Therefore, white light emitting material can be synthesized by using the appropriate doping concentrations of Eu, Tb, and Gd in the material. Thus, $Gd_{77.82}Eu_{9.92}Tb_{12.26}$ doped complex was prepared and it is isostructural to complexes **2**-**4** (Fig. S1, ESI†). The fluorescent spectrum of the doped complex was recorded. The doped complex simultaneously shows the characteristic emission peaks of the Eu(III) and the Tb(III) ions and a broad ligand emission band as shown in Fig. 4. Interestingly, under excitation at 280 nm, the CIE chromaticity coordinate (0.328, 0.300) (Fig. 4, Inset) is close to the standard white light (0.333, 0.333) according to 1931 CIE coordinate diagram[14]. The color rendering index and correlated color temperature for the white light (0.328, 0.300) are 81 and 5760K, respectively.

It is noted that Sm(III) complex **1** provides blue (434nm), green (563), orange (598 nm), and red (644 nm) light, as it is possible to realize white light emission though the doping of luminescent Ln(III) ions into the Sm(III) - complex, when a suitable blue, green to red intensity ratio. Unfortunately, complex **1** is not isomorphous to complexes **2** and **3**, which can not make doped material for white light emission.

3.3 Up-conversion luminescence

Up-conversion materials have attracted significant attention as potential solid state visible lasers and biological labels[5]. In this paper, the $Gd_{90.52}Yb_{5.89}Er_{3.59}$ doped complex was prepared and it is isostructural to complexes **2**, **5** and **6** (Fig. S1, ESI†). Up-conversion luminescence of the doped complex is discussed. The up-conversion emission bands of the $Gd_{90.52}Yb_{5.89}Er_{3.59}$ material are at 412 nm, 527-550 nm, and 653 nm (Fig. 5). The proposed up-conversion mechanism is described in the energy diagram, as shown in Fig. 6. In $Gd_{90.52}Yb_{5.89}Er_{3.59}$ doped complex, the lowest excited level ($^6P_{7/2}$) of Gd(III) is far higher than excited levels of Yb(III) and Er(III), energy transfer from Yb(III) and Er(III) to Gd(III) can be avoided. So, up-conversion mechanism for Gd(III)

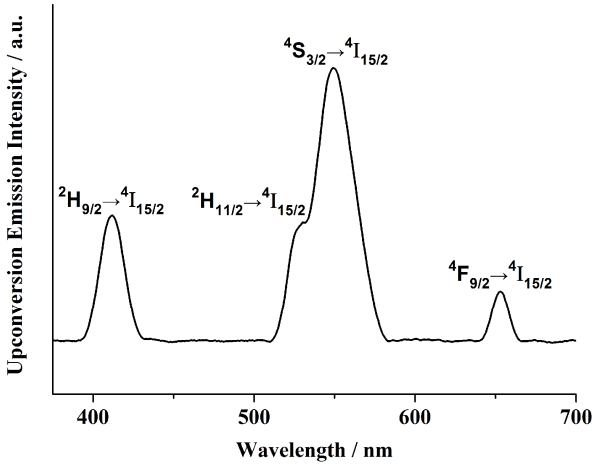

Fig. 5 Up-conversion emission for the Er(III) ion in the $Gd_{90.52}Yb_{5.89}Er_{3.59}$ doped complex.

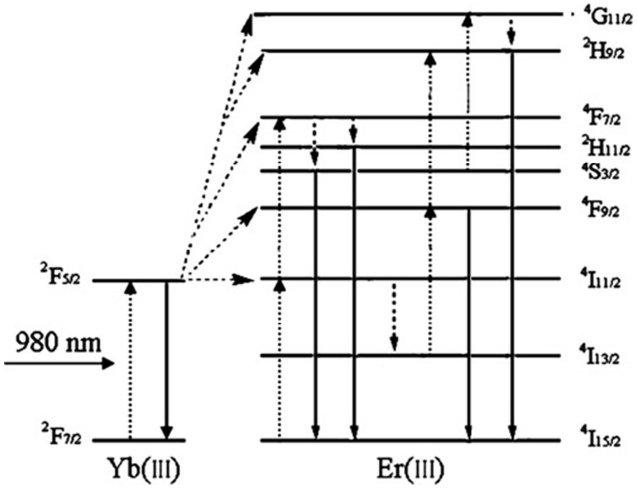

Fig. 6 Up-conversion mechanism of the Gd:Er,Yb codoped complex under 980nm excitation at room temperature. The solid lines represent emission process, while the dashed lines represent photon excitation or nonradiative relaxation.

doped system is essentially the same ones as in Y(III) doped system.[2j] When excited at 980 nm, the Yb(III) at the ground state $^2F_{7/2}$ absorbs the photon to excited state $^2F_{5/2}$. Then the energy can be transferred to Er(III) ion and the Er(III) ion at ground state $^4I_{11/2}$ transits to excited state $^4F_{7/2}$. Subsequently, non-radiative relaxations from this state populate the $^2H_{11/2}$ and $^4S_{3/2}$ states. Then the radiative transitions of the $^2H_{11/2} \rightarrow {}^4I_{15/2}$ and $^4S_{3/2} \rightarrow {}^4I_{15/2}$ generate the strong emission at 527-550 nm in the green spectral region. Red up-conversion luminescence at 653 nm can occur either following: Er(III) at $^4F_{9/2}$ state is populated from the $^4S_{3/2}$ state by non-radiative relaxations; Non-radiative relaxations from $^4I_{11/2}$ state populate the $^4I_{13/2}$ state, which transits to the $^4F_{9/2}$ state via asecond-photon. Then, the radiative transition of the $^4F_{9/2} \rightarrow {}^4I_{15/2}$ at 653 nm is produced. Weak blue emission at 412 nm results from energy transfer $^2H_{9/2} \rightarrow {}^4I_{15/2}$ transition. The $^2H_{9/2}$ state is populated through the third photon absorption of the $^4F_{9/2}$ ground state. Furthermore, some of Er(III) ions in the $^4S_{3/2}$ state are transferred into $^4G_{11/2}$ state by the third photon absorption,

followed by non-radiative relaxations to $^2H_{9/2}$ state, leading to emission from $^2H_{9/2}$ to $^4I_{15/2}$.

3.4 Thermogravimetric analysis (TGA)

Complexes **1-6** and $Gd_{77.82}Eu_{9.92}Tb_{12.26}$ and $Gd_{90.52}Yb_{5.89}Er_{3.59}$ doped complexes do not contain guest molecules, the TGA study (Fig. S5, ESI†) shows no weight loss from room temperature to about 270 °C, indicating the thermal stability of the framework. The weight loss between 270 and 550 °C should be attributed to the decomposition of the organic ligands. The final mass remnant is roughly consistent with a deposition of corresponding oxides.

Conclusions

The first examples of LnOFs containing H_2N-BDS have been designed and synthesized. Sm(III) complex is a 3D pillared-layer structure constructed from $[SmO_6N_2]$ polyhedra by the SO_3 group, H_2N-BDS and ox ligands while Eu(III), Gd(III), Tb(III), Er(III) and Yb(III)- complexes possess 2D frameworks constructed from $[LnO_4N_4]$ polyhedra by H_2N-BDS and ox ligands. Sm(III), Eu(III), Gd(III), and Tb(III) - complexes display different luminescence behavior due to their quite different energy level diagrams. Gd(III) ion has high energy of the lowest emitting level, which could be useful in the design of DC or UC doped emitting materials. Eu(III)/Tb(III) complexes are promising candidates because of the characteristic red/green emission. Interestingly, a combination of Gd(III), Tb(III) and Eu(III) complexes in appropriate ratio produces a white light emission. A significant UC emission blue (410 nm), green (518-570 nm), and red (656 nm) for Gd:Yb,Er doped complex is observed.

Acknowledgement

The authors are grateful to the National Natural Science Foundation of China (21071101), Beijing Municipal Science & Technology Commission (Z131103002813097) and Scientific Research Base Development Program of the Beijing Municipal Commission of Education.

Notes and references

Beijing Key Laboratory for Optical Materials and Photonic Devices, Deparment of Chemistry, Capital Normal University, Beijing 100048. Fax: +86 10 68902320; Tel: +86 10 68902320; E-mail: xiali@mail.cnu.edu.cn

† Electronic Supplementary Information (ESI) available: [details of any supplementary information available should be included here]. See DOI: 10.1039/b000000x/

1. (a) Jean-Claude G. Bünzli, *Chem. Rev.*, 2010, **110**, 2729; (b) Y. Li, S. S. Zhang, and D. T. Song, *Angew. Chem. Int. Ed.*, 2013, **52**, 710; (c) E. Brunet, O. Juanes, J. C. Rodriguez-Ubis, *Curr. Chem. Biol.*, 2007, **1**, 11; (d) J. Kido, Y. Okamoto, *Chem. Rev.*, 2002, **102**, 2357; (e) L. D. Carlos, R. A. S. Ferreira, V. de Z. Bermudez, and S. J. L. Ribeiro, *Adv. Mater.*, 2009, **21**, 509.

2. (a) S. Song, X. Li and Y. H. Zhang, *Dalton Trans.*, 2013, **42**, 10409; (b) Y. H. Zhang, X. Li and S. Song, *Chem. Commun.*, 2013, **49**, 10397; (c) H. B. Zhang, X. C. Shan, L. J. Zhou, P. Lin, R. F. Li, E. Ma, X. G. Guo, S. W. Du, *J. Mater. Chem. C*, 2013, **1**, 888; (d) S. Dang, J. H. Zhang, Z. M. Sun, *J. Mater. Chem.*, 2012, **22**, 8868; (e) D. F. Sava, L. E. S. Rohwer, M. A. Rodriguez, T. M. Nenoff, *J. Am. Chem. Soc.*, 2012, **134**, 3983; (f) Z. F. Liu, M. F. Wu, S. H. Wang, F. K. Zheng, G. E. Wang, J. Chen, Y. Xiao, A. Q. Wu, G. C. Guo, J. S. Huang, *J. Mater. Chem. C*, 2013, **1**, 4634; (g) S. L. Zhong, R. Xu, L. F. Zhang, W. G. Qu, G. Q. Gao, X. L. Wu, A. W. Xu, *J. Mater. Chem.*, 2011, **21**, 16574; (h) X. T. Rao, Q. Huang, X. L. Yang, Y. J. Cui, Y. Yang, C. D. Wu, B. L. Chen, G. D. Qian, *J. Mater. Chem.*, 2012, **22**, 3210; (i) K. Liu, H. P. You, Y. H. Zheng, G. Jia, Y. J. Huang, M. Yang, Y. H. Song, L. H. Zhang, H. J. Zhang, *Cryst. Growth Des.*, 2010, **10**, 16; (j) X. Ma, J. Tian, H. Y. Yang, K. Zhao, X. Li, *J. Solid State Chem.*, 2013, **201**, 172.

3. (a) E. F. Schubert and J. K. Kim, *Science*, 2005, **308**, 1274; (b) C. Feldmann, T. Jüstel, C. R. Ronda and P. J. Schmidt, *Adv. Funct. Mater.*, 2003, **13**, 511; (c) H. A. Höppe, *Angew. Chem., Int. Ed.*, 2009, **48**, 3572; (d) E. Downing, L. Hesselink, J. Ralston and R. Macfarlane, *Science*, 1996, **273**, 1185; (e) T. Jüstel, H. Nikol and C. Ronda, *Angew. Chem., Int. Ed.*, 1998, **37**, 3084; (f) Y. Zou, T. L. Ye, D. G. Ma, J. G. Qin and C. L. Yang, *J. Mater. Chem.*, 2012, **22**, 23485; (g) L. D. Carlos, R. A. S. Ferreira, V. D. Bermudez, B. Julian-Lopez and P. Escribano, *Chem. Soc. Rev.*, 2011, **40**, 536; (h) K. Zhang, Z. Chen, C. L. Yang, Y. Zou, S. L. Gong, Y. T. Tao, J. G. Qin and Y. Cao, *J. Mater. Chem.*, 2008, **18**, 3366; (i) Y. J. Cui, H. Xu, Y. F. Yue, Z. Y. Guo, J. C. Yu, Z. X. Chen, J. K. Gao, Y. Yang, G. D. Qian and B. L. Chen, *J. Am. Chem.Soc.*, 2012, **134**, 3979.

4. (a) C. Lin, M.T. Berry, R. Anderson, S. Smith, P.S. May, *Chem. Mater.*, 2009, **21**, 3406; (b) H. Schäfer, P. Ptacek, H. Eickmeier, M. Haase, *Adv. Funct. Mater.*, 2009, **19**, 3091; (c) D. F. Weng, X. J. Zheng, L. P. Jin, *Eur. J. Inorg. Chem.*, 2006, 4184; (d) D. F. Weng, X. J. Zheng, X.-B. Chen, L. C. Li, L. P. Jin, *Eur. J. Inorg. Chem.*, 2006, **45**, 3410.

5. (a) F. Auzel, *Chem. Rev.,* 2004, **104**, 139; (b) H. S. Mader, P. Kele, S. M. Saleh and O. S. Wolfbeis, *Curr. Opin. Chem. Biol.*, 2010, **14**, 582. (c) Z. G. Chen, H. L. Chen, H. Hu, M. X. Yu, F. Y. Li, Q. Zhang, Z. G. Zhou, T. Yi, and C. H. Huang, *J. Am. Chem. Soc.*, 2008, **130**, 3023; (d) G. F.Wang, Q. Peng, and Y. D. Li, *Acc. Chem. Res.*, 2011, **44**, 322.

6. B. L. Chen, Y. Yang, F. Zapata, G. D. Qian, Y. S. Luo, J. H. Zhang and E. B. Lobkovsky, *Inorg. Chem.*, 2006, **45**, 8882.

7. (a) M. Gudenschwager and M. S. Wickleder, *Z. Anorg. Allg. Chem.*, 2012, 1567; (b) T. W. T. Muesmann, J. Ohlert, M. S. Wickleder and J. Christoffers, *Eur. J. Org. Chem.*, 2011, 1695.

8. G. Accorsi, A. Listorti, K. Yoosaf and N. Armaroli, *Chem. Soc. Rev.*, 2009, **38**, 1690.

9. (a) G.M. Sheldrick, SHELXTL Version 5.1, Bruker Analytical X-ray Instruments Inc., Madison, Wisconsin, USA, 1998. (b) G.M. Sheldrick, SHELX-97, PC Version, University of Göttingen, Germany, 1997.

10. V. A. Blatov, L. Carlucci, G. Ciani and D. M. Proserpio, *CrystEngComm*, 2004, **6**, 377.

11. L. Armelaoa, S. Quici, F. Barigelletti, G. Accorsic, G. Bottaro, M. Cavazzini and E. Tondello, *Coord. Chem. Rev.*, 2010, **254**, 487.

12.(a) Q. C. Sheng, Y. L. Shen, S. Liu, W. T. Li and D. P. Chen, *Appl. Phys. Lett.*, 2012, **101**, 061904; (b) R. Feng, L. Chen, Q. H. Chen, X. C. Shan, Y. L. Gai, F. L. Jiang and M. C. Hong, *Cryst. Growth Des.*, 2011, **11**, 1705.

13. (a) P. C. R. Soares-Santos, L. Cunha-Silva, F. A. A. Paz, R. A. S. Ferreira, J. Rocha, L. D. Carlos, H. I. S. Nogueira, *Inorg. Chem.*, 2010, **49**, 3428. (b) Viswanathan, S.; Bettencourt-Dias, A. D. *Inorg. Chem.*, 2006, **45**, 10138.

14. T. Smith; J. Guild, *Trans Opt. Soc.*, 1931, **33**, 73.